Symmetry Breaking and Silver in Gold Nanorod Growth

Michael J. Walsh,*,† Steven J. Barrow,‡,∥ Wenming Tong,‡ Alison M. Funston,‡ and Joanne Etheridge†,§

†Department of Materials Engineering, ‡School of Chemistry, and §Monash Centre for Electron Microscopy, Monash University, VIC, 3800, Australia.
∥Present address: (S.J.B.): Department of Chemistry, Cambridge University, Cambridge, UK.

ABSTRACT Formation of anisotropic nanocrystals from isotropic single-crystal precursors requires an essential symmetry breaking event. Single-crystal gold nanorods have become the model system for investigating the synthesis of anisotropic nanoparticles, and their growth mechanism continues to be the subject of intense investigation. Despite this, very little is known about the symmetry breaking event that precedes shape anisotropy. In particular, there remains limited understanding of how an isotropic seed particle becomes asymmetric and of the growth parameters that trigger and drive this process. Here, we present direct atomic-scale observations of the nanocrystal structure at the embryonic stages of gold nanorod growth. The onset of asymmetry of the nascent crystals is observed to occur only for single-crystal particles that have reached diameters of 4−6 nm and only in the presence of silver ions. In this size range, small, asymmetric truncating surfaces with an open atomic structure become apparent. Furthermore, {111} twin planes are observed in some immature nanorods within 1−3 monolayers of the surface. These results provide direct observation of the structural changes that break the symmetry of isotropic nascent nanocrystals and ultimately enable the growth of asymmetric nanocrystals.

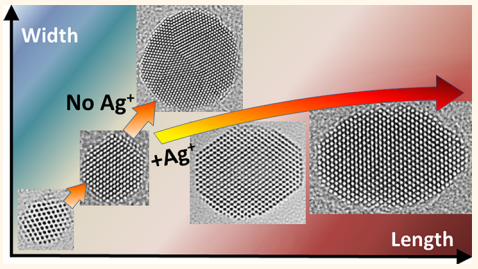

KEYWORDS: symmetry breaking · gold nanorods · anisotropic growth

Shape anisotropy has become a powerful tool in tuning the structure−property relationships of nanoparticles. Various empirically derived surfactant-driven wet chemistry techniques now enable a high degree of shape control in colloidal nanoparticle synthesis. However, a key question remains, namely, what triggers an isotropic seed particle, with a cubic lattice, to grow at different rates along symmetry equivalent directions? To achieve this, an initial symmetry breaking event must occur and is a prerequisite for anisotropic growth.

Perhaps the most widely studied anisotropic nanoparticle system is that of single-crystal gold nanorods, in which the aspect ratio (nanoparticle length/width) of the nanorod can be used to tune the longitudinal localized surface plasmon resonance (LSPR) from the visible to near-infrared wavelengths.[1] This has attracted significant interest for applications within optoelectronics,[2−4] catalysis,[5,6] biosensing,[7−9] drug and gene delivery,[10,11] and photothermal hyperthermia treatments,[12,13] where the LSPR can be shifted to infrared frequencies in the biologically transparent window.

The size, shape, and surfaces of nanoparticles can now often be controlled through surfactant-driven synthesis techniques. In the case of single-crystal gold nanorods, the most widely used synthesis method is that of Ag^+-assisted seed-mediated growth in the presence of specific cationic surfactants containing halide counterions—commonly, cetyltrimethylammonium bromide (CTAB).[14] The nanoparticles synthesized using this method are single crystals with aspect ratios up to ∼4, which have recently been reported to be bound by high-index side facets[15,16] and in other cases by low-index facets.[17] There is currently little agreement as to the mechanism by which single-crystal gold nanorod growth takes place. A major obstacle in obtaining clear insights into the surfactant-driven growth mechanism is the number of possible variables that could be involved. These include the relative concentrations of $HAuCl_4$, CTAB, $AgNO_3$, and ascorbic acid, the size, structure, and concentration of seed particles, solution pH, and the many possible synergistic effects of the aforementioned. Although many of

* Address correspondence to michael.j.walsh@monash.edu.

Received for review October 28, 2014 and accepted January 8, 2015.

Published online January 08, 2015
10.1021/nn506155r

these factors can now be placed in a general framework for Au nanoparticle synthesis,[18,19] the question as to what causes an initially isotropic single-crystal seed particle to break symmetry remains.

It is generally accepted that a halide-containing cationic surfactant, such as CTAB, is crucial for Au nanorod growth, while there is substantial empirical evidence that Ag^+ is an essential ingredient for the formation of single-crystal nanorods.[1,14] However, there is little direct evidence as to what role either Ag^+ or other surfactants play in the embryonic stages of crystal growth and therefore what drives symmetry breaking of the nascent crystals.

The limited experimental observations of gold nanorod growth at the *symmetry breaking* stage have meant that proposed mechanisms have remained largely speculative. It has been suggested that CTAB micelles may act as soft templates to guide shape anisotropy,[20−22] and this is largely supported by the correlation of expected surface facet and micelle size at the symmetry breaking point. However, direct evidence for such a process is lacking, and questions such as why the resulting uniform crystal shape and growth direction and what is the role of Ag^+ remain unresolved.

Alternatively, if a selective surface passivation mechanism, such as capping of specific surfaces by AgBr complexes[23−25] or by Ag underpotential deposition[26−28] is responsible for symmetry breaking, how does this lead to shape anisotropy? A conventional cuboctahedral structure is a single crystal bound by 8 {111} and 6 {100} facets[29]—arranged symmetrically—meaning there is no obvious reason for asymmetric growth. If growth is inhibited on the {100} surfaces but allowed on the {111} facets, the resulting particle morphology would be a cube bound by {100} surfaces (as shown schematically in Supporting Information Figure S1), and indeed, this is a commonly observed byproduct of nanorod synthesis. Clearly, greater insight at the atomic scale into the anisotropic structural evolution of seed particles is needed.

An obvious question is "where is the silver"? Due to the overlapping X-ray peaks and the extremely low concentrations, silver is difficult to detect on Au nanoparticles. Only very recently[30] has energy-dispersive X-ray (EDX) spectroscopy managed to detect silver in statistically significant amounts on fully grown nanorods, and in this case, a special, optimized geometry for X-ray detection was required. The particles analyzed in the present study are not amenable to meaningful EDX analysis of silver content (see Supporting Information).

Here we present a systematic study of the atomic structure of gold nanoparticles as a function of variable growth parameters at the embryonic stages of gold nanorod synthesis. First, aberration-corrected transmission electron microscopy (TEM) is used to characterize the atomic structure of small Au seed particles that are used to nucleate growth. The seed particles are then overgrown slightly, both with and without the addition of silver ions, and these are characterized. Finally, nanocrystals were analyzed at the early stages of nanorod growth in order to provide insights into the continuing growth process following the onset of anisotropy. We observe that there is a critical size threshold at which the nascent nanocrystals become asymmetric and identify key structural changes that occur at this size. We show that silver is essential to break the symmetry of the embryonic nanocrystals and for the subsequent formation of single-crystal Au nanorods. The evolving structure of the growing seed particle and the role of silver are discussed as key steps in the symmetry breaking process of single-crystal gold nanorod growth.

Aberration-corrected phase contrast TEM and annular dark-field scanning transmission electron microscopy (ADF STEM) are popular methods for imaging atomic structures at the highest resolution. ADF STEM image contrast depends in part on atomic number and thickness and can therefore be used to obtain three-dimensional information about the particle, provided that certain experimental parameters are quantified.[17,31,32] However, for the small nanoparticles considered here, the highly localized electron dose from a focused STEM probe leads to excessive atom movement and changes to particle orientation and even structure on a time scale shorter than typical acquisition times and, as such, is not best suited to the current study. The small size of nanoparticles at the embryonic stages of growth makes them inherently less stable than fully grown nanorods under prolonged exposures to an intense electron beam needed for chemical mapping. In addition, sample cleaning procedures such as ligand exchange, centrifuging, and plasma cleaning are required but may not be desired or possible. For these reasons, we have chosen to use aberration-corrected phase contrast TEM imaging to characterize both the initial and overgrown seed particles as it allows fast acquisition with controlled exposure of the particle to the electron beam. However, it is not generally possible to deduce the facet orientations from inspection of these two-dimensional phase contrast images, unless it is known there is a coherent facet parallel to the electron beam direction or there exists a plausible morphological model which can be tested by comparing the experimental image with images simulated using that model. In this work, surface facets are only assigned where these conditions have existed.

RESULTS

Characterization of Initial Seed Particles. We begin the study with the characterization of the atomic structure of the initial seed particles. The addition of surfactants is thought to modify nanoparticle surface energetics

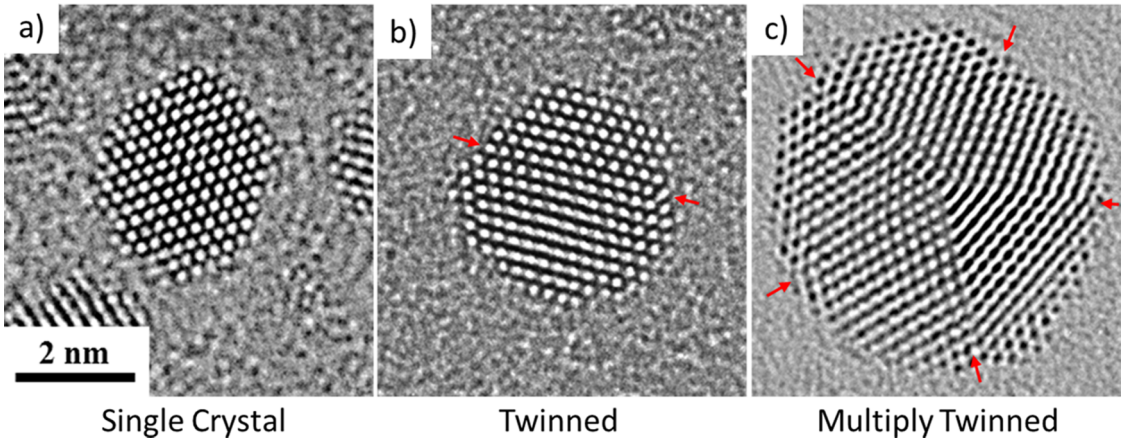

Figure 1. Au seed particles synthesized in CTAB are predominantly single crystal (a), with a small percentage twinned (b) or multiply twinned (c) (as indicated by the arrows).

and, therefore, the resulting minimum energy morphology. It is therefore important to characterize the atomic structure of initial seed particles with their appropriate surfactant environment (in this case, CTAB).

The small gold seed particles utilized in this synthetic method have previously been reported to be single crystals following stabilization by alkanethiol ligands.[26] Here, the seeds were analyzed as synthesized, that is, without ligand exchange and therefore with CTAB as the ligand to avoid any structural effects on these small particles from the ligand exchange. Figure 1a shows a typical single-crystal cuboctahedral seed particle. Much more than half of the seed particles synthesized in CTAB are observed to be single-crystal structures, although small numbers of twinned (b) and multiply twinned particle (MTP) structures (c) are also observed. A more accurate statistical analysis of particle morphology distributions cannot be achieved because the determination of morphology requires comparison of images of particles aligned close to the zone axis with simulations. Only a subset of particles falls near this orientation. Single-crystal seeds that fulfill these conditions were identified as cuboctahedra.

The cuboctahedron is a very well-known and well-characterized single-crystal structure and is predicted by the Wulff model to be the minimum energy structure for a face-centered cubic metal such as gold.[29,33] However, for gold particles in the absence of surfactants, the minimum free energy structure in the size range of <10 nm is multiply twinned,[34−36] for which the preferred inclusion of lower-energy {111} surface facets leads to inherently strained structures such as icosahedra and decahedra.[36,37] However, surfactants such as CTAB adsorb to the surface of the particle and may therefore modify the surface energetics, causing the minimum energy structure of the particle to differ from that expected based on conventional thermodynamic considerations. The prevalence of cuboctahedra particles in the presence of CTAB suggests that the surfactant modifies the surface energetics of the particle by reducing the energy of {100} surfaces relative to the {111} surface, thereby removing the driving force for the formation of multiply twinned particles that can incorporate a higher fraction of {111} surfaces at the expense of elastic strain and consequently modifying the minimum energy structure away from the multiply twinned icosahedra and decahedra. Calculations based on other surfactant systems, such as ionic liquids, support this, reporting nearly equal thermodynamic stabilities of {111}, {100}, and {110} surfaces.[24,28]

The inherent instability of small nanoparticles under the electron beam means that the illuminating radiation can potentially induce atomic movement, resulting in modifications to the surfaces and internal structure of the nanoparticle. Such effects must be carefully analyzed in order to ensure high fidelity in particle structure characterization, and details of this analysis are reported in the Supporting Information. For the small (~2 nm) seed particles, beam-induced transitions from single crystal to MTP structures (Figure S2) meant that an accurate statistical analysis of particle yield was not possible. However, the slightly larger nanoparticles discussed in the following results showed significantly improved stability under the electron beam, with no overall shape or structure transitions occurring during the short acquisition times used. This therefore allows for accurate characterization of particle size, structure, and surface faceting.

Characterization of Slightly Overgrown Seeds. In a standard nanorod synthesis, seed particles such as those shown in Figure 1 are used as nucleation points for nanorod growth *via* their addition to a growth solution containing $HAuCl_4$, CTAB, $AgNO_3$, and ascorbic acid. Here, an intermediary step is added to this procedure in order to investigate the so far elusive mechanism by which symmetry breaking occurs. In this step, the seed crystals are overgrown in a growth solution containing only enough gold ions to increase the size of the seed

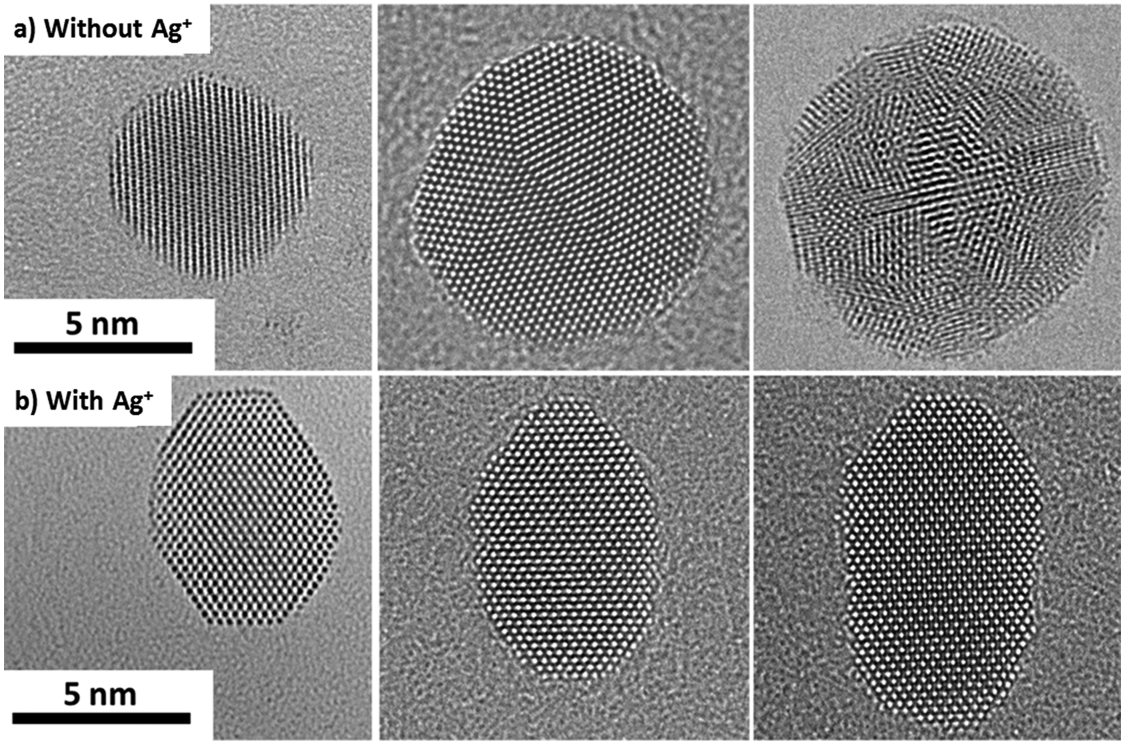

Figure 2. (a) Gold seed particles overgrown in the absence of Ag^+ remain spherical and may become twinned or multiply twinned. (b) Au seeds overgrown in the presence of Ag^+ (63.4 μM of $AgNO_3$) are observed to become anisotropic.

nanoparticles by a few nanometers. Within these growth solutions, the concentration of the silver ion (and consequently the ratio of silver to gold) is varied. The full synthetic procedure is reported in the Methods section; however, it is important to note that the concentration of CTAB in these growth solutions is characteristic of conditions commonly used for spherical overgrowth of seeds and is lower than used for typical nanorod synthesis, while still being above the critical micelle concentration. The visible spectra measured for the seeds overgrown with and without the presence of the Ag^+ ion are shown in Figure S4. In addition to the surface plasmon resonance associated with spherical particles, the addition of $AgNO_3$ leads to the development of a second peak at longer wavelengths, consistent with the development of shape anisotropy within the sample—for nanorods, this resonance is due to the longitudinal localized surface plasmon resonance. This lower-energy resonance is not observed for samples grown in the absence of silver ion.

Aberration-corrected TEM analysis shows that seed particles overgrown without Ag^+ remain approximately spherical. Of the seeds overgrown in the presence of Ag^+, over a third have broken symmetry and grown anisotropically to an aspect ratio of >1.25. Examples of this are shown in Figure 2, in which the anisotropic growth direction is seen to be ⟨100⟩, known to be the final length axis for single-crystal gold nanorods.

A summary of the size, shape, and crystal structure of seed particles overgrown both without Ag^+ and in the presence of 12.7 and 63.4 μM of $AgNO_3$ is shown in Figure 3, based on the individual analysis of 36−50 particles for each overgrowth condition. For the purpose of this analysis, each particle is defined as having a major axis (D_{major}), measured as the longest axis of the particle, and a minor axis (D_{minor}), measured orthogonally to D_{major}. The aspect ratio of a given particle is therefore D_{major}/D_{minor}. From Figure 3a, it can be seen that, for particles overgrown in 12.7 and 63.4 μM of $AgNO_3$, symmetry breaking occurs at particle diameters of 4−6 nm, while effectively no anisotropic growth is observed for seeds overgrown in the absence of Ag^+. All particles that undergo symmetry breaking and anisotropic growth are single-crystal structures, and any twinned or multiply twinned particles remain approximately spherical.

Seeds overgrown in the absence of Ag^+ begin to incorporate an increasing number of twins and other defects, such as stacking faults, as they increase in size, with the percentage of single-crystal structures dropping from approximately 85% (for $D < 6$ nm) to 50% (for $D > 6$ nm), with a quarter of the larger overgrown particles incorporating multiple twin planes.

Overgrowth in the presence of Ag^+ proceeds more slowly,[19] presumably allowing a more epitaxial deposition of gold atoms and helping to maintain the initial seed particle crystal structure during growth. This significantly reduces the number of particles with twin planes or stacking faults relative to those observed during the growth of Au seeds without Ag^+, as shown

in Figure 3b. However, an increase in the proportion of multiply twinned particles is observed when the $AgNO_3$ concentration is increased from 12.7 to 63.4 μM.

The seemingly stochastic nature of the symmetry breaking event[38] is highlighted by the observation that under these overgrowth conditions in the presence of silver, and accounting for any twinned or defective structures, around half the particles within the 4−6 nm range remain approximately spherical. Given the high yield of nanorod structures in the final growth product, it is fair to assume that these single-crystal particles would go on to break symmetry if allowed to continue to grow, and therefore, their presence enables studies of particles in the embryonic stages of growth before symmetry breaking has occurred.

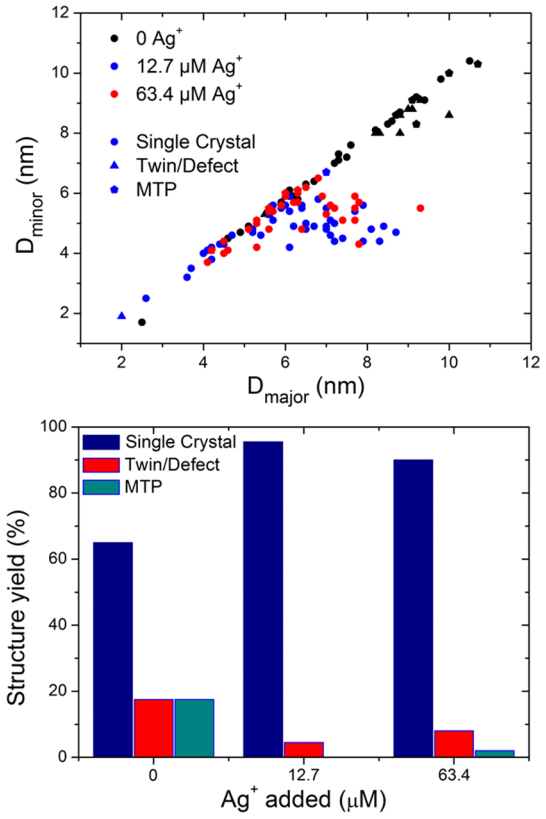

Figure 3. Overgrown Au seed particle size and structure for different concentrations of added Ag^+. Structure yields for particles grown in the presence of 0, 12.7, and 63.4 μM of $AgNO_3$ are based on analysis of 40, 50, and 36 particles, respectively.

Figure 4 shows two cuboctahedral seed particles—overgrown in the presence of 63.4 μM of $AgNO_3$—approximately 4 nm in diameter and orientated in the ⟨011⟩ direction. It is expected that the facet orientations of cuboctahedral seed particles will be {111} and {100},[29] and the geometry of this two-dimensional image is consistent with this. However, in addition to these facets, some small higher-index asymmetric truncations are also observed; that is, the edge where the two nominal {111} planes would meet is replaced by a plane face parallel to the ⟨110⟩ direction (which is not necessarily smooth at the atomic level). (Note that more accurate determination of the percentage of nanoparticles with truncations is not feasible. In certain crystallographic projections (such as [001]), a truncating facet is not readily distinguishable from an edge between two facets, while particles imaged away from a zone axis are not suitable for facet determination. When suitable projection conditions are met, a majority of single-crystal particles in the 4−6 nm range show some level of truncation on at least one edge where {111} facets would otherwise meet.

Notably, these truncations tend to occur asymmetrically. Such truncating facets may be initially incorporated into the cuboctahedral structure to remove edge effects where lower-index facets would otherwise meet. At this small size, the non-negligible contribution of under-coordinated edge and corner atoms has a significant effect on the overall particle-free energy,[39] and therefore, the incorporation of a higher-index truncating surface may be energetically favorable to a sharp atomic edge. These facets are absent in the classical cuboctahedral structure and provide an alternative type of surface with a different expected interaction with the surfactant and adsorbate species. Also particularly notable is the close correlation of the size at which truncations in the single-crystal seed structure appear and the particle size at which symmetry breaking is observed.

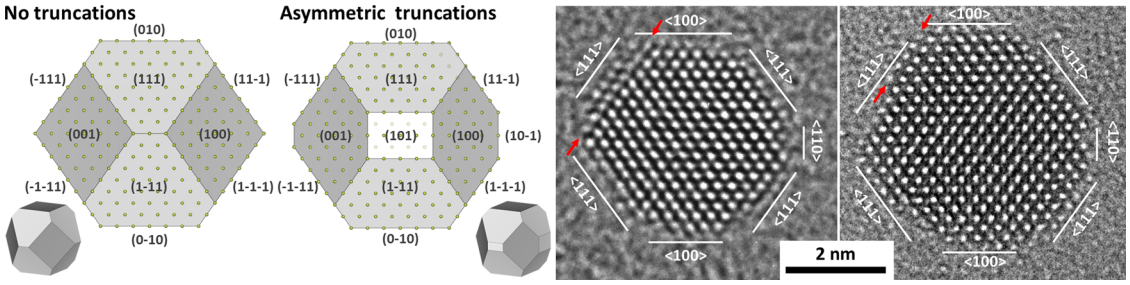

Figure 4. Particle models (left) of a perfect cuboctahedra and a cuboctahedra incorporating asymmetric {110} truncations. TEM images (right) of Au seed particles overgrown in the presence of 63.4 μM $AgNO_3$. The single-crystal particles closely match the asymmetrically truncated cuboctahedral model, with some small truncations parallel to the ⟨110⟩ direction. Arrows indicate additional atoms in twinned sites. Particle models created using Vesta.[40]

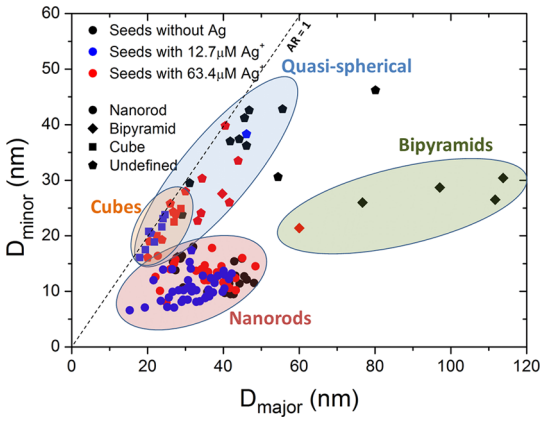

Figure 5. Nanoparticle products following growth of overgrown seeds in CTAB and Ag^+.

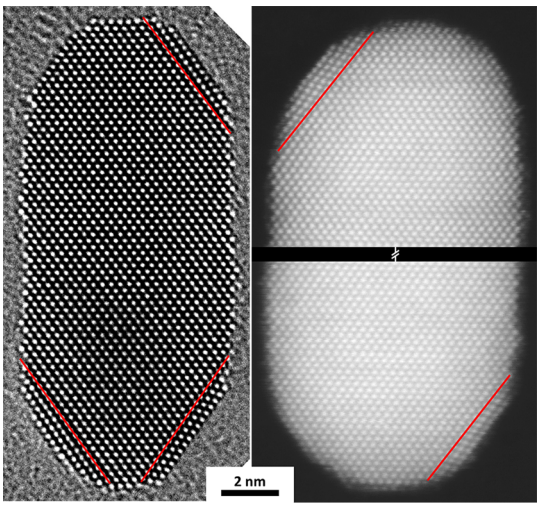

Figure 6. Twin planes observed parallel to the bridging facets of gold nanorods grown directly from seed. TEM image of a Au nanorod after 6 min of growth (left) and ADF STEM images of the tips of a nanorod after 20 min of growth (right). (Red lines delineate the twin plane boundary.)

Kinetic effects and the dynamic nanoscale growth environment may well give rise to such small truncations. However, in the absence of Ag^+, any truncations are always sub-nanometer in size, whereas in the presence of Ag^+, surfaces approximately parallel with {110}-type direction range from small truncations of a few atoms to extended facets, which grow with the length of the nanoparticle. We may surmise then that it is only in the presence of Ag^+ that the higher-index truncations are stabilized and therefore able to grow into larger facets.

In addition to the development of some truncating facets, another feature of both particles shown in Figure 4 is the appearance of adatoms or even adlayers that are deposited in twinned as opposed to single-crystal sites (as indicated by arrows). In a separate experiment described later, we also observe twin planes in some immature Au nanorods at the early stages of nanorod synthesis using established methods[14] (see Methods section).

Characterization of Final Growth Products from Overgrown Seeds. The final synthesis products of overgrown seeds in a standard nanorod growth solution are shown in Figure 5 and Supporting Information Figures S5 and S6. All nanorods are observed to be single crystals, while the byproducts tend to be bipyramids (in agreement with Liu and Guyot-Sionnest[26]), cubes or other quasi-spherical shapes. The final growth products from seeds overgrown in 12.7 μM of Ag^+ have the highest yield of nanorods, significantly reducing the number of large quasi-spherical byproducts that are often twinned or pentatwinned. This corresponds well with the increased number of MTPs observed for seeds overgrown in 63.4 μM of Ag^+. As well as affecting the final aspect ratio of nanorods, the amount of Ag^+ added clearly determines symmetry breaking and the final yield of nanorods and other byproducts.

Characterization of Twin Planes at Early Stages of Nanorod Synthesis. In a separate experiment, we characterized nanorods at different stages of a standard seed-mediated nanorod synthesis (*i.e.*, without the seed overgrowth step) by removing samples from the growth solution at regular time intervals, in a similar approach to that employed by Park *et al.*[20] For this nanorod synthesis, the general trend of the various stages of growth is consistent with those reported,[20] albeit slightly faster, with anisotropic growth leading to nanorods *via* an intermediate dumbbell-type structure.

Atomic level characterization of particles grown for 6 and 20 min in the nanorod growth solution is shown in Figure 6 and reveals the inclusion of twin planes in the growing nanorod. This is particularly surprising given that the final nanorod products were observed to be single crystals, as is normal for this synthesis. While twin planes are by no means ubiquitous in the intermediate nanorod structure, they do offer further insights into the mechanism of nanorod growth, as will be explored in the discussion to follow.

The twins are observed to be along the {111} plane and typically lie about three atomic layers from the surface. The energy for twin formation in Au is known to be very small[41] and can easily occur due to the kinetics of nanoparticle growth. As the final nanorod product is a perfect single crystal, any twin planes must be removed before the end of the growth process. The twin planes terminate close to or at the point at which the bridging facet meets the side facet (Figure 6). It is likely that atoms can occupy twin sites in incomplete surface layers parallel to the {111} plane with minimal energy cost. However, following further Au atom deposition, these layers become complete and interact with facets at the side and the tip, at which point the twin causes a loss of atomic ordering at these edges, providing a driving force for atomic rearrangement to create a perfect single-crystal structure. This structural change is observed in two sequential image frames

taken 14 s apart, shown in Figure S7, with the electron beam likely providing sufficient energy to overcome the energy barrier for atomic movement. Atoms in a surface layer parallel to {111} initially occupy twinned sites, causing a loss of atomic ordering at the corners of both the tip and side facets (arrowed). The surface layer shifts to form perfect single-crystal atomic sites *via* a simple glide mechanism, leading to coherent interfaces at the edges where the facets meet.

DISCUSSION

Toward an Understanding of Symmetry Breaking. The results presented here make three key observations regarding symmetry breaking: first, that it is only following the crucial addition of Ag^+ that anisotropic growth begins; second, that symmetry breaking occurs for single-crystal particles at diameters of 4−6 nm; and finally, in this size range, small asymmetric truncations are observed to appear on the seed particles. Furthermore, {111} twin planes are observed in some seed particles and immature nanorods within 1−3 monolayers of the surface.

Consider first the observation of small truncations, which is the first direct observation of a change in atomic structure in the growing seed particle. Atomic resolution images of seed particles in the same size range that symmetry breaking occurs but before the onset of anisotropy (Figure 4) are consistent with a cuboctahedral structure with {111} and {100} facets, except that some small truncations parallel to ⟨110⟩ can also be present. These presumably arise to remove edges that would otherwise make a significant contribution to the total surface energy of the particle.

The particles shown in Figure 4 are approximately 4 nm in diameter and have developed small truncations of between 4 and 6 atoms across. It is remarkable that the particle size at which small truncations are first observed matches the size at which symmetry breaking occurs, as shown experimentally in Figures 2 and 3. This critical size may be related to the minimum size at which truncating facets can be incorporated into the particle structure. Furthermore, *if* silver is playing a role in stabilizing this truncation—which is plausible given its more open, rough atomic structure—then there may be a minimum truncation size capable of adsorbing and becoming stabilized by a silver layer, which in turn helps define the minimum particle size for which symmetry breaking can occur.

The development of truncating facets provides an alternative surface of a more open atomic structure that is expected to have different surfactant and adsorbate interactions and therefore growth rates relative to the lower index, more close-packed {111} and {100} surfaces. However, to generate anisotropy, such alternative surfaces must be incorporated nonsymmetrically in the particle structure in order to give a preferential growth direction. This can possibly be explained by the dynamic

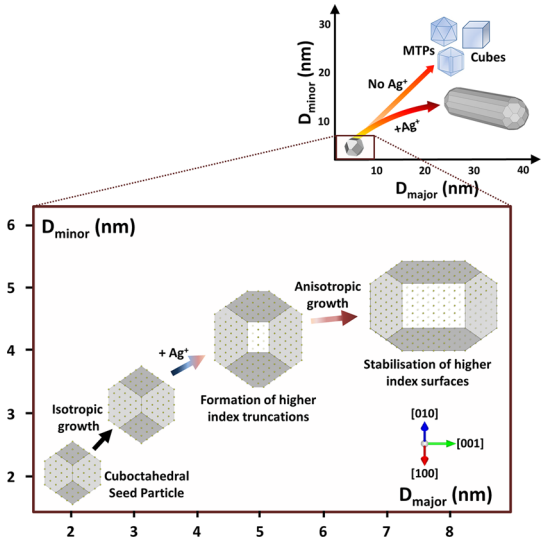

Figure 7. Schematic representation of the proposed key steps of the symmetry breaking process in single-crystal gold nanorod growth. Particle models created using VESTA.[40]

nature of nanoparticle growth, in which small truncations may develop nonuniformly in the growing seed particle, as seen in Figure 4.

If these truncations are stabilized by a passivating Ag layer, their enhanced stability relative to other surfaces would mean that growth proceeds more rapidly in other directions, with the initial truncation becoming a side facet of the growing single-crystal nanorod. The relatively rapid creation and stabilization of such surfaces followed by anisotropic growth might lead to what has previously been reported as a seemingly stochastic "popcorn"-like symmetry breaking mechanism,[38] resulting in a large distribution of particle sizes observed during the first few minutes of nanorod synthesis. Indeed, the particles shown in Figure 2 can be thought of as elongated versions of those seen in Figure 4 following anisotropic growth, with the truncations becoming side facets in the growing nanorod. The surface faceting may continue to evolve during further nanorod growth.[15,16,20]

These observations suggest some key steps in the symmetry breaking process that gives rise to anisotropic growth and the resulting single-crystal gold nanorods. These proposed steps are represented schematically in Figure 7 and described below:

(1) Seed particles synthesized in CTAB are single crystals with a cuboctahedral morphology, bound by symmetrically arranged {111} and {100) surfaces.
(2) Upon introduction to a Ag^+-assisted gold nanorod growth solution, the seed particles initially grow isotropically until reaching a critical particle diameter of 4−6 nm.
(3) At this point, small truncating surfaces consisting of a few atoms across form nonuniformly at the intersection of {111} facets. These truncations

may be atomically rough and lie approximately parallel with ⟨110⟩. They are of a more open atomic structure than the comparatively close-packed {111} and {100} surfaces already present in the nanoparticle, and as such are potentially preferred sites for Ag underpotential deposition.

(4) Stabilization of the higher-index truncations prevents further Au atom deposition. Growth proceeds on the lower-index surfaces, leading to the truncations becoming side facets in the growing embryonic nanorod structure.

The observation of twin planes and partial surface layers in twin sites parallel to the {111} plane suggests that it is the {111} surface facets that are the preferred site for Au atom deposition. Continued growth on the {111} bridging facets would explain the formation of dumbbell-like morphologies at intermediate stages of nanorod synthesis, observed both here and previously by Park *et al.*[20] Also noteworthy is that the incorporation of a twin plane is in itself inherently a symmetry breaking event. Bipyramids formed as a byproduct in the same growth solution grow up to five times the size of the nanorods, showing that particle morphologies with a high proportion of {111} facets grow to much larger sizes than those with higher-index surfaces, consistent with Au deposition and growth taking place predominantly on {111} facets.

The sensitivity of anisotropic growth to the size and structure of the seed particle is presumably due to the existence of multiple surface types, which have differing interaction energies with the surfactants. Figure 3 shows that, as gold seeds are grown larger in the absence of Ag^+, the relatively fast reduction of Au ions and subsequent deposition means that defects such as stacking faults or twin planes may be incorporated into the seed particle, which in turn has a deleterious effect on the final yield of nanorods. Therefore, the use of small seed particles that can be introduced to a Ag^+-containing growth solution at the earliest stage of growth is important to maintain their single crystallinity before the symmetry breaking event can occur. The role of Ag^+ in selectively passivating higher-index surfaces is consistent with the reduction of MTPs with the addition of 12.7 μM of $AgNO_3$. As the $AgNO_3$ concentration is increased to 63.4 μM, the number of MTPs increases, suggesting that additional Ag^+ also passivates the lower-index {111} surfaces, reducing the driving force for single-crystal structures. This then causes the observed drop in nanorod yield after growth seen in Figure S6.

CONCLUSIONS

In summary, we show that small facet truncations develop in the growing seed structure and that it is the stabilization of these truncations in the presence of Ag^+ that leads to asymmetry in the nascent nanocrystals. We also observe, in some cases, {111} twin planes in seed particles and developing nanorods. These observations suggest several key steps in the process of symmetry breaking in gold nanorod growth.

METHODS

Hexadecyltrimethylammonium bromide (98%) was purchased from Ajax Finechem. Sodium borohydride (99%), gold(III) chloride trihydrate, and L-ascorbic acid were purchased from Sigma-Aldrich. Silver nitrate was purchased from Merck. Ultrapure water (milli-Q) was used for the preparation of all solutions.

Gold Seeds. Aqueous solutions of CTAB (4.700 mL, 0.1 M) and $HAuCl_4$ (0.025 mL, 0.05 M) were mixed and allowed to stir for at least 5 min. Following this, freshly prepared aqueous $NaBH_4$ (0.300 mL. 0.025M) was rapidly added into the mixture under rigorous stirring to form a brownish yellow solution. The resulting solution was stirred for 15 min and kept at 29 ± 1 °C for 40 min.

Growth of Gold Nanorods from Gold Seeds. Aqueous solutions of CTAB (10 mL, 0.1 M) and $HAuCl_4$ (0.100 mL, 0.05 M) were mixed and allowed to stir for at least 5 min. Aqueous solutions of freshly prepared ascorbic acid (0.075 mL, 0.1 M) and silver nitrate (0.080 mL, 0.01 M) were then sequentially added with thorough mixing following each addition. Finally, gold seeds (0.050 mL) were added with stirring. The color of the solution gradually changed within 2 min. The final solution was held at 29 ± 1 °C for 20 min.

Overgrowth of Gold Seeds. Aqueous solutions of CTAB (1.500 mL, 0.1 M), milli-Q water (10.000 mL), and $HAuCl_4$ (0.020 mL, 0.05 M) were mixed and allowed to stir for at least 5 min. An aqueous solution of freshly prepared ascorbic acid (0.020 mL, 0.1 M) was then added, and following complete mixing, the solution changed from yellow to colorless. Aqueous silver nitrate solution (0, 0.016, and 0.080 mL, 0.01 M) was then added. Finally, the gold seed solution (1.000 mL) was added to the above mixture under stirring. The solution became colored, indicative of the formation of nanorods, within 10 s. The resulting nanorod solution was grown at 29 ± 1 °C for 30 min.

Growth of Gold Nanorods from Overgrown Gold Seeds. Aqueous solutions of CTAB (10.00 mL, 0.1 M) and $HAuCl_4$ (0.100 mL, 0.05 M) solutions were mixed and allowed to stir for at least 5 min. An aqueous solution of freshly prepared ascorbic acid (0.075 mL, 0.1 M) was then added, and following complete mixing, the solution changed from yellow to colorless. Aqueous silver nitrate (0, 0.016, and 0.080 mL, 0.01 M) was then added. Finally, the overgrown seed solution (0.500 M) was added to the above mixture under stirring. The solution became colored, indicative of the formation of nanorods, within 2 min. The resulting nanorod solution was grown at 29 ± 1 °C for 120 min.

Following each synthesis step, a sample of the growth solution was taken and immediately dropped onto an ultrathin (<3 nm) carbon support on a Cu TEM grid for electron microscopy analysis. Fully grown nanorods were centrifuged before being deposited on a TEM grid. Examples of nanorods at intermediate stages of growth shown in Figure 6 were prepared by a conventional nanorod synthesis route, that is, without the seed overgrowth step. Following deposition, the TEM grid was washed in high-purity ethanol in order to remove excess CTAB. There was no plasma cleaning of the samples prior to electron microscopy analysis.

Electron microscopy was carried out at the Monash Centre for Electron Microscopy on a FEI Titan^3 80-300 kV FEGTEM equipped with both probe and imaging spherical aberration correctors. All imaging was carried out at 300 kV and at room temperature, with the exception of Figure S3, which was acquired at 80 kV and near liquid nitrogen temperature. All images are unfiltered, with some small adjustments to contrast

and brightness levels. UV−vis spectra were acquired using a Cary 60 UV−vis spectrophotometer.

Conflict of Interest: The authors declare no competing financial interest.

Acknowledgment. This work was supported by the Australian Research Council (ARC) Grant DP120101573 and used microscopes at the Monash Centre for Electron Microscopy funded by ARC Grant LE0454166. The authors thank Dr. Hadas Katz-Boon, Dr. Matthew Weyland, and Prof. Paul Mulvaney for helpful discussions.

Supporting Information Available: Synthesis conditions and additional figures. This material is available free of charge *via* the Internet at http://pubs.acs.org.

REFERENCES AND NOTES

1. Pérez-Juste, J.; Pastoriza-Santos, I.; Liz-Marzán, L. M.; Mulvaney, P. Gold Nanorods: Synthesis, Characterization and Applications. *Coord. Chem. Rev.* **2005**, *249*, 1870–1901.
2. Zijlstra, P.; Chon, J. W. M.; Gu, M. Five-Dimensional Optical Recording Mediated by Surface Plasmons in Gold Nanorods. *Nature* **2009**, *459*, 410–413.
3. Barrow, S. J.; Funston, A. M.; Wei, X.; Mulvaney, P. DNA-Directed Self-Assembly and Optical Properties of Discrete 1D, 2D and 3D Plasmonic Structures. *Nano Today* **2013**, *8*, 138–167.
4. Funston, A. M.; Gómez, D. E.; Karg, M.; Vernon, K. C.; Davis, T. J.; Mulvaney, P. Aligned Linear Arrays of Crystalline Nanoparticles. *J. Phys. Chem. Lett.* **2013**, *4*, 1994–2001.
5. Wu, B.; Zheng, N. Surface and Interface Control of Noble Metal Nanocrystals for Catalytic and Electrocatalytic Applications. *Nano Today* **2013**, *8*, 168–197.
6. Novo, C.; Funston, A. M.; Mulvaney, P. Direct Observation of Chemical Reactions on Single Gold Nanocrystals Using Surface Plasmon Spectroscopy. *Nat. Nanotechnol.* **2008**, *3*, 598–602.
7. Jain, P. K.; Huang, X.; El-Sayed, I. H.; El-Sayed, M. A. Noble Metals on the Nanoscale: Optical and Photothermal Properties and Some Applications in Imaging, Sensing, Biology, and Medicine. *Acc. Chem. Res.* **2008**, *41*, 1578–1586.
8. Huang, X.; Neretina, S.; El-Sayed, M. A. Gold Nanorods: From Synthesis and Properties to Biological and Biomedical Applications. *Adv. Mater.* **2009**, *21*, 4880–4910.
9. Anker, J. N.; Hall, W. P.; Lyandres, O.; Shah, N. C.; Zhao, J.; Van Duyne, R. P. Biosensing with Plasmonic Nanosensors. *Nat. Mater.* **2008**, *7*, 442–453.
10. Salem, A. K.; Searson, P. C.; Leong, K. W. Multifunctional Nanorods for Gene Delivery. *Nat. Mater.* **2003**, *2*, 668–671.
11. Mura, S.; Nicolas, J.; Couvreur, P. Stimuli-Responsive Nanocarriers for Drug Delivery. *Nat. Mater.* **2013**, *12*, 991–1003.
12. Huang, X.; El-Sayed, I. H.; Qian, W.; El-Sayed, M. A. Cancer Cell Imaging and Photothermal Therapy in the Near-Infrared Region by Using Gold Nanorods. *J. Am. Chem. Soc.* **2006**, *128*, 2115–2120.
13. von Maltzahn, G.; Centrone, A.; Park, J.-H.; Ramanathan, R.; Sailor, M. J.; Hatton, T. A.; Bhatia, S. N. SERS-Coded Gold Nanorods as a Multifunctional Platform for Densely Multiplexed Near-Infrared Imaging and Photothermal Heating. *Adv. Mater.* **2009**, *21*, 3175–3180.
14. Nikoobakht, B.; El-Sayed, M. A. Preparation and Growth Mechanism of Gold Nanorods (NRs) Using Seed-Mediated Growth Method. *Chem. Mater.* **2003**, *15*, 1957–1962.
15. Katz-Boon, H.; Rossouw, C. J.; Weyland, M.; Funston, A. M.; Mulvaney, P.; Etheridge, J. Three-Dimensional Morphology and Crystallography of Gold Nanorods. *Nano Lett.* **2011**, *11*, 273–278.
16. Carbó-Argibay, E.; Rodríguez-González, B.; Gómez-Graña, S.; Guerrero-Martínez, A.; Pastoriza-Santos, I.; Pérez-Juste, J.; Liz-Marzán, L. M. The Crystalline Structure of Gold Nanorods Revisited: Evidence for Higher-Index Lateral Facets. *Angew. Chem., Int. Ed.* **2010**, *49*, 9397–9400.
17. Goris, B.; Bals, S.; Van den Broek, W.; Carbó-Argibay, E.; Gómez-Graña, S.; Liz-Marzán, L. M.; Van Tendeloo, G. Atomic-Scale Determination of Surface Facets in Gold Nanorods. *Nat. Mater.* **2012**, *11*, 930–935.
18. Personick, M. L.; Mirkin, C. A. Making Sense of the Mayhem Behind Shape Control in the Synthesis of Gold Nanoparticles. *J. Am. Chem. Soc.* **2013**, *135*, 18238–18247.
19. Langille, M. R.; Personick, M. L.; Zhang, J.; Mirkin, C. A. Defining Rules for the Shape Evolution of Gold Nanoparticles. *J. Am. Chem. Soc.* **2012**, *134*, 14542–14554.
20. Park, K.; Drummy, L. F.; Wadams, R.; Koerner, H.; Nepal, D.; Fabris, L.; Vaia, R. A. Growth Mechanism of Gold Nanorods. *Chem. Mater.* **2013**, *25*, 555–563.
21. Wadams, R. C.; Fabris, L.; Vaia, R. A.; Park, K. Time-Dependent Susceptibility of the Growth of Gold Nanorods to the Addition of a Cosurfactant. *Chem. Mater.* **2013**, *25*, 4772–4780.
22. Jana, N. R. Gram-Scale Synthesis of Soluble, Near-Monodisperse Gold Nanorods and Other Anisotropic Nanoparticles. *Small* **2005**, *1*, 875–882.
23. Hubert, F.; Testard, F.; Spalla, O. Cetyltrimethylammonium Bromide Silver Bromide Complex as the Capping Agent of Gold Nanorods. *Langmuir* **2008**, *24*, 9219–9222.
24. Almora-Barrios, N.; Novell-Leruth, G.; Whiting, P.; Liz-Marzán, L. M.; López, N. Theoretical Description of the Role of Halides, Silver, and Surfactants on the Structure of Gold Nanorods. *Nano Lett.* **2014**, *14*, 871–875.
25. Niidome, Y.; Nakamura, Y.; Honda, K.; Akiyama, Y.; Nishioka, K.; Kawasaki, H.; Nakashima, N. Characterization of Silver Ions Adsorbed on Gold Nanorods: Surface Analysis by Using Surface-Assisted Laser Desorption/Ionization Time-of-Flight Mass Spectrometry. *Chem. Commun.* **2009**, *0*, 1754–1756.
26. Liu, M.; Guyot-Sionnest, P. Mechanism of Silver(I)-Assisted Growth of Gold Nanorods and Bipyramids. *J. Phys. Chem. B* **2005**, *109*, 22192–22200.
27. Personick, M. L.; Langille, M. R.; Zhang, J.; Mirkin, C. A. Shape Control of Gold Nanoparticles by Silver Underpotential Deposition. *Nano Lett.* **2011**, *11*, 3394–3398.
28. Jha, K. C.; Liu, H.; Bockstaller, M. R.; Heinz, H. Facet Recognition and Molecular Ordering of Ionic Liquids on Metal Surfaces. *J. Phys. Chem. C* **2013**, *117*, 25969–25981.
29. Henry, C. R. Morphology of Supported Nanoparticles. *Prog. Surf. Sci.* **2005**, *80*, 92–116.
30. Jackson, R.; McBride, J. R.; Rosenthal, S. J.; Wright, D. W. Where's the Silver? Imaging Trace Silver Coverage on the Surface of Gold Nanorods. *J. Am. Chem. Soc.* **2014**, *136*, 5261–5263.
31. Dwyer, C.; Maunders, C.; Zheng, C. L.; Weyland, M.; Tiemeijer, P. C.; Etheridge, J. Sub-0.1 nm-Resolution Quantitative Scanning Transmission Electron Microscopy without Adjustable Parameters. *Appl. Phys. Lett.* **2012**, *100*, 191915.
32. Katz-Boon, H.; Rossouw, C. J.; Dwyer, C.; Etheridge, J. Rapid Measurement of Nanoparticle Thickness Profiles. *Ultramicroscopy* **2013**, *124*, 61–70.
33. Wulff, G. *Z. Kristallogr. Mineral.* **1901**, *34*, 449.
34. Marks, L. D. Surface Structure and Energetics of Multiply Twinned Particles. *Philos. Mag. A* **1984**, *49*, 81–93.
35. Barnard, A. S.; Young, N. P.; Kirkland, A. I.; van Huis, M. A.; Xu, H. F. Nanogold: A Quantitative Phase Map. *ACS Nano* **2009**, *3*, 1431–1436.
36. Howie, A.; Marks, L. D. Elastic Strains and the Energy-Balance for Multiply Twinned Particles. *Philos. Mag. A* **1984**, *49*, 95–109.
37. Walsh, M. J.; Yoshida, K.; Kuwabara, A.; Pay, M. L.; Gai, P. L.; Boyes, E. D. On the Structural Origin of the Catalytic Properties of Inherently Strained Ultrasmall Decahedral Gold Nanoparticles. *Nano Lett.* **2012**, *12*, 2027–2031.
38. Edgar, J. A.; McDonagh, A. M.; Cortie, M. B. Formation of Gold Nanorods by a Stochastic "Popcorn" Mechanism. *ACS Nano* **2012**, *6*, 1116–1125.
39. Campbell, C. T.; Parker, S. C.; Starr, D. E. The Effect of Size-Dependent Nanoparticle Energetics on Catalyst Sintering. *Science* **2002**, *298*, 811–814.

40. Momma, K.; Izumi, F. VESTA 3 for Three-Dimensional Visualization of Crystal, Volumetric and Morphology Data. *J. Appl. Crystallogr.* **2011**, *44*, 1272–1276.
41. Ringe, E.; Van Duyne, R. P.; Marks, L. D. Kinetic and Thermodynamic Modified Wulff Constructions for Twinned Nanoparticles. *J. Phys. Chem. C* **2013**, *117*, 15859–15870.